A theoretical model for single-molecule incoherent scanning tunneling spectroscopy

2008 J. Phys.: Condens. Matter 20 445004

(http://iopscience.iop.org/0953-8984/20/44/445004)

J. Phys.: Condens. Matter **20** (2008) 445004 (6pp) doi:10.1088/0953-8984/20/44/445004

A theoretical model for single-molecule incoherent scanning tunneling spectroscopy

H Raza

NSF Network for Computational Nanotechnology and School of Electrical and Computer Engineering, Purdue University, West Lafayette, IN 47907, USA
and
School of Electrical and Computer Engineering, Cornell University, Ithaca, NY 14853, USA

E-mail: hr89@cornell.edu

Received 8 February 2008, in final form 28 July 2008
Published 25 September 2008
Online at stacks.iop.org/JPhysCM/20/445004

Abstract
Single-molecule scanning tunneling spectroscopy (STS), with dephasing due to elastic and inelastic scattering, is of some current interest. Motivated by this, we report an extended Hückel theory (EHT)-based mean-field non-equilibrium Green's function (NEGF) transport model with electron–phonon scattering treated within the self-consistent Born approximation (SCBA). Furthermore, a procedure based on EHT basis set modification is described. We use this model to study the effect of the temperature-dependent dephasing due to low lying modes in the far-infrared range for which $\hbar\omega \ll k_B T$, on the *resonant* conduction through the highest occupied molecular orbital (HOMO) level of a phenyl dithiol molecule bonded to fcc-Au(111) contact. We finally propose to include dephasing in room temperature molecular resonant conduction calculations.

(Some figures in this article are in colour only in the electronic version)

1. Introduction

We present an extended Hückel theory (EHT)-based self-consistent mean-field transport model for incoherent single-molecule spectroscopy. Although simple, this approach is worth pursuing because EHT is numerically inexpensive and overcomes many of the shortcomings of the more sophisticated theories [1] and has been used for nanoelectronics [2, 3]. Furthermore, the simplicity and the exponential dependence of the Slater type orbital basis set allows an intuitive solution to tip modeling as described in this paper. The proper tip modeling is important because if condensed matter like short-ranged orbitals are used, one has to bring the tip very close to the molecule (about 4–5 Å) to obtain the experimentally observed current levels. This artificially results in higher than the actual voltage drop across the molecule, resulting in not only the wrong Laplace potential but the Hartree potential is also overestimated and the image potentials are wrong.

Furthermore, the electron–phonon scattering in molecular structures on different metallic substrates has been studied quite extensively at low temperature experimentally [4–8] and theoretically [9–15] in the form of off-resonant inelastic tunneling spectroscopy (IETS). In IETS, the molecule acts as the scattering region and the distinct peaks in the second derivative of I–V characteristics identify the molecular vibrations. Moreover, in electron–phonon scattering, not only does the electron exchange energy with the phonon bath but also its phase is irreversibly lost due to the phonon's degree of freedom. If the phonon energy ($\hbar\omega$) is less than a characteristic energy (e.g. $k_B T$), this inelastic dephasing process may be approximated by an elastic dephasing event for numerical convenience. Since all the energy channels are coupled in inelastic dephasing, solving for it is computationally challenging.

Apart from this, the phonon modes of a molecule bonded to a substrate are different from the gas phase. Organic molecules in the gas phase have vibrational energies in the infrared range, i.e. 100–350 meV. However, experiments using IETS [6], high resolution electron energy-loss spectroscopy (HREELS) [15] and low temperature transport [16] suggest

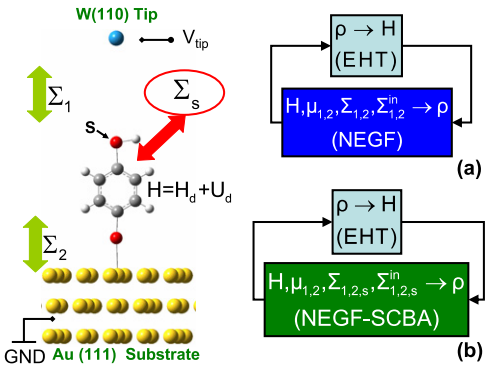

Figure 1. Schematic diagram. Scanning tunneling spectroscopy (STS) set-up for probing conduction through a phenyl/benzene dithiol (PDT/BDT) molecule bonded to an Au(111) substrate. Voltage is applied at the tungsten W(110) tip. (a) A schematic showing the self-consistent procedure of solving EHT-NEGF equations for coherent transport [22]. (b) A schematic detailing the self-consistent procedure of solving EHT-NEGF-SCBA equations for quantum transport with elastic and inelastic dephasing.

that bonding to a substrate leads to low lying modes in the far-infrared range. Dominant modes having vibrational energies less than about 10 meV have been reported theoretically [10, 11]. These far-infrared modes are the result of the combined motion of the molecule with respect to the contacts. Most of these infrared modes are longitudinal modes and couple well with carriers [10, 11]. Hence, the low lying modes, for which $\hbar\omega \ll k_B T$ at room temperature, are the most important phonon modes for molecules bonded to substrates. Dephasing due to these modes could be high due to the large phonon population for $\hbar\omega \ll k_B T$, whereas phonon modes in the infrared range are expected to have a subtle dephasing effect due to the small phonon population. In a previous study [17], we report transport calculations at room temperature for a styrene chain bonded to an n^{++}-H:Si(001) substrate. In [17], we propose to include dephasing due to low lying modes in order to theoretically reproduce experimental results.

Furthermore, in the context of molecular spectroscopy, there are four sources of broadening: (1) contact broadening which is about 0.1–0.3 eV for a good contact, (2) the Fermi function broadening of the two contacts, (3) broadening due to Hartree self-consistency which is usually small in the STS set-up due to the tip being about 1 nm away from the substrate and (4) broadening due to electron–phonon scattering which is temperature-dependent due to the phonon population given by the Bose–Einstein factor as $1/[\exp(\hbar\omega/k_B T) - 1]$. The main focus of this work is the broadening due to this fourth source in transport through a phenyl/benzene dithiol (PDT/BDT) molecule bonded to an Au(111) substrate as shown in figure 1. The tip configuration used is tungsten W(110) having a work function of about 5.2 eV.

This paper is divided into five sections. In section 2, we describe the mean-field self-consistent EHT-NEGF-SCBA model for studying transport with dephasing due to electron–phonon scattering. Furthermore, details are provided about the electrostatic calculation. Tip modeling is an important aspect of the calculations and is discussed in section 3. In section 4, we discuss the results and report the temperature dependence of the transport quantities on the electron–phonon scattering due to low lying modes. Finally, we provide conclusions in section 5. The molecular visualization is done using GaussView [18].

2. Formalism and theoretical model

We use the single-particle non-equilibrium Green's function formalism (NEGF) in the mean-field approximation using a non-orthogonal basis to model the quantum transport. We define the time-retarded non-equilibrium Green's function in a non-orthogonal basis as [19, 20]

$$G(E, V_{\text{tip}}) = [(E + \mathrm{i}0^+)S - H - E_{fc}S - \Sigma_{1,2} - \Sigma_{\text{s}}]^{-1} \quad (1)$$

where S is the overlap matrix and $H = H_d + U_d$. H_d is the device Hamiltonian for an isolated molecule expressed in EHT [21]. $\Sigma_{1,2}$ are the self-energies of W(110) tip and Au(111) contact, respectively—calculated recursively using EHT as well. Since there is no vacuum reference in EHT parametrization, we use the input from experiments or other sophisticated theoretical methods to set the reference. E_{fc} is used as a parameter to achieve this objective. It is taken as 2 eV in this paper to match the experimentally observed peak in the conductance spectrum [29]. U_d incorporates both the Laplace potential due to the applied tip voltage (V_{tip}) and the Hartree potential due to the non-equilibrium density of electrons in the molecular channel. The contact self-energies $\Sigma_{1,2}$ are related to the broadening functions as $\Gamma_{1,2} = \mathrm{i}(\Sigma_{1,2} - \Sigma_{1,2}^{\dagger})$. The tip self-energy ($\Sigma_1$) is further discussed in section 3. The Au(111) self-energy (Σ_2) has been discussed in [22]. The spectral function is defined as $A = \mathrm{i}(G - G^{\dagger})$, which is related to the density of states of the molecular region as $\text{DOS}(E) = 2(\text{for spin}) \times \text{tr}(AS)/2\pi$. The electron correlation function $G^n (= -\mathrm{i}G^<)$ is given as

$$G^n = G(\Sigma_1^{\text{in}} + \Sigma_2^{\text{in}} + \Sigma_{\text{s}}^{\text{in}})G^{\dagger} \quad (2)$$

where $\Sigma_{1,2}^{\text{in}} (= -\mathrm{i}\Sigma_{1,2}^<)$ are the contact inflow functions defined as $\Gamma_{1,2} f_{1,2}$ and $\Sigma_{\text{s}}^{\text{in}} (= -\mathrm{i}\Sigma_{\text{s}}^<)$ is the scattering inflow function. $f_{1,2}(E)$ are the contact Fermi functions given as $1/[1 + \exp((E - \mu_{1,2})/k_B T)]$. $\mu_{1,2}$ are the chemical potentials of the two contacts given as $\mu_1 = \mu_o - eV_{\text{tip}}$ and $\mu_2 = \mu_o$ respectively—μ_o is the equilibrium chemical potential. In this model, contacts are assumed to remain in equilibrium. This is a valid assumption for metallic contacts and degenerately doped semiconducting contacts. However, for the moderately doped or lightly doped semiconducting contacts, band bending due to V_{tip} makes these calculations computationally expensive. The hole correlation function is defined as $G^p = A - G^n$. The electron density matrix is then given as

$$\rho = \frac{1}{2\pi} \int_{-\infty}^{\infty} \mathrm{d}E\, G^n(E). \quad (3)$$

The total number of electrons is computed as $N = 2(\text{for spin}) \times \text{tr}(\rho S)$. Finally, the I–V characteristics are

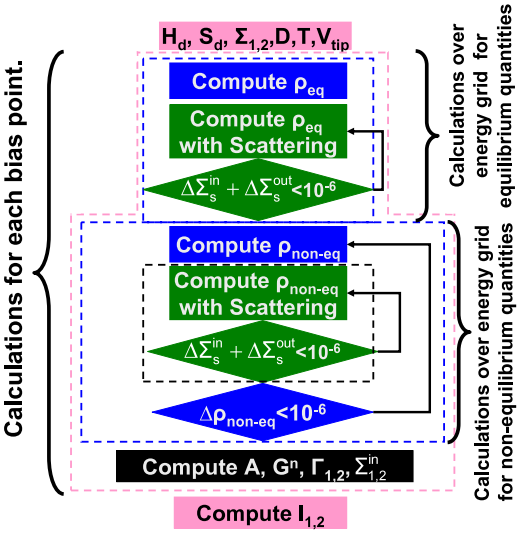

Figure 2. Block diagram for incoherent transport. For elastic dephasing, all the energy channels are independent. Therefore, energy-dependent quantities can be calculated independently for each energy point with the convergence criteria shown. Equilibrium and non-equilibrium quantities for each bias point are calculated as shown. The blocks are color coded (online only) to match with the blocks in figures 1(a) and (b). For inelastic dephasing, since energy channels are coupled, one has to use convergence criteria on the calculated energy-dependent quantities over the whole energy range.

computed as follows [19, 23]:

$$I_i(V_{\rm tip}) = 2(\text{for spin}) \times \frac{e}{h}\int_{-\infty}^{\infty} \mathrm{d}E\ \mathrm{tr}(\Sigma_i^{\rm in}A - \Gamma_i G^n). \quad (4)$$

Since scattering self-energy ($\Sigma_{\rm s}$), G, G^n and $\Sigma_{\rm s}^{\rm in}$ depend on each other, we solve these four quantities self-consistently along with the Hartree self-consistent loop as shown in figure 1(b). The flow diagram for the self-consistent procedure at each bias is shown in figure 2. For SCBA, it can be analytically shown that the current through the *scattering contact* is always zero.

The scattering inflow function ($\Sigma_{\rm s}^{\rm in}$), outflow function ($\Sigma_{\rm s}^{\rm out}$) and broadening function ($\Gamma_{\rm s}$) are defined as [24]

$$\Sigma_{\rm s}^{\rm in}(E) = \int_0^{\infty} \frac{\mathrm{d}(\hbar\omega)}{2\pi}[D^{\rm em}(\hbar\omega)SG^n(E+\hbar\omega)S + D^{\rm ab}(\hbar\omega)SG^n(E-\hbar\omega)S] \quad (5)$$

$$\Sigma_{\rm s}^{\rm out}(E) = \int_0^{\infty} \frac{\mathrm{d}(\hbar\omega)}{2\pi}[D^{\rm em}(\hbar\omega)SG^p(E-\hbar\omega)S + D^{\rm ab}(\hbar\omega)SG^p(E+\hbar\omega)S] \quad (6)$$

$$\Gamma_{\rm s}(E) = \Sigma_{\rm s}^{\rm in} + \Sigma_{\rm s}^{\rm out} = \int_0^{\infty} \frac{\mathrm{d}(\hbar\omega)}{2\pi} \times (D^{\rm em}(\hbar\omega)S[G^n(E+\hbar\omega) + G^p(E-\hbar\omega)]S + D^{\rm ab}(\hbar\omega)S[G^n(E-\hbar\omega) + G^p(E+\hbar\omega)]S) \quad (7)$$

where $D^{\rm em}(\hbar\omega) = (N+1)D_o(\hbar\omega)$ and $D^{\rm ab}(\hbar\omega) = N\,D_o(\hbar\omega)$ are the emission and absorption dephasing functions, respectively. N is the equilibrium number of phonons given by Bose–Einstein statistics as $1/[\exp(\hbar\omega/k_{\rm B}T) - 1]$. Equation (5) implies that electron inflow at a particular energy E is dependent on the electron correlation function G^n at energy $E + \hbar\omega$ for emission and $E - \hbar\omega$ for absorption. This relationship is reversed for the electron outflow as in equation (6). The overall broadening due to this scattering process is given by $\Gamma_{\rm s}(E)$. Furthermore, $D_o(\hbar\omega)$ is a fourth-ranked tensor and is related to the electron–phonon interaction potential (U) as $\langle i, j|U^{\dagger}U|k, l\rangle$. Thus, $D_o(\hbar\omega)$ can be different for different molecular orbitals and is explicitly written as $D_o(i, j; k, l; \hbar\omega)$. Equations (5)–(7) are modified from those reported in [24] for a non-orthogonal basis as discussed in [20].

High energy phonon limit: for $\hbar\omega \gg k_{\rm B}T$, $N \approx 0$ and $N + 1 \approx 1$, hence $D^{\rm em} \approx D_o$ and $D^{\rm ab} \approx 0$. Thus, equation (7) becomes

$$\Gamma_{\rm s}(E) = \int_0^{\infty} \frac{\mathrm{d}(\hbar\omega)}{2\pi} D_o(\hbar\omega)S[G^n(E+\hbar\omega) + G^p(E-\hbar\omega)]S. \quad (8)$$

Therefore, the contribution due to absorption is negligible in this case because not enough phonons are available to be absorbed. Moreover, since $\Gamma_{\rm s}(E)$ is temperature-independent, the broadening due to electron–phonon scattering for $\hbar\omega \gg k_{\rm B}T$ is approximately temperature-independent.

Low energy phonon limit: for $\hbar\omega \ll k_{\rm B}T$, by keeping the first term in the Taylor series expansion of $\exp(\hbar\omega k_{\rm B}T) \approx 1 + \hbar\omega/k_{\rm B}T$, one obtains $N + 1 \approx N \approx k_{\rm B}T/\hbar\omega$. This leads to

$$\Gamma_{\rm s}(E) = \int_0^{\infty} \frac{\mathrm{d}(\hbar\omega)}{2\pi}[D^{\rm em}(\hbar\omega) + D^{\rm ab}(\hbar\omega)]SA(E)S \quad (9)$$

and

$$D^{\rm em}(\hbar\omega) \approx D^{\rm ab}(\hbar\omega) = N\,D_o(\hbar\omega) \approx \frac{k_{\rm B}T}{\hbar\omega}D_o(\hbar\omega). \quad (10)$$

We finally obtain $\Gamma_{\rm s}(E)$ as

$$\Gamma_{\rm s}(E) \approx \underbrace{T\int_0^{\infty} \frac{\mathrm{d}(\hbar\omega)}{2\pi}\frac{2k_{\rm B}D_o(\hbar\omega)}{\hbar\omega}}_{D} SA(E)S \quad (11)$$

where D is referred to as dephasing strength. As shown above, the broadening due to elastic dephasing is directly proportional to temperature.

Furthermore, the real part of $\Sigma_{\rm s}(E)$ is computed by taking a Hilbert transform of the imaginary part as below:

$$\Sigma_{\rm s}(E) = \frac{1}{\pi}\int_{-\infty}^{\infty} \mathrm{d}y \frac{-\Gamma_{\rm s}(y)/2}{E-y} - \mathrm{i}\Gamma_{\rm s}(E)/2. \quad (12)$$

Calculating the real part of $\Sigma_{\rm s}(E)$ is computationally expensive and leads to convergence issues. Previously, it has been reported [12] that this real part contributes of the order of meV. We therefore ignore it in this paper. We phenomenologically approximate the dephasing strength (D) by a constant. This approximation treats T_1 and T_2 time in an average manner and seems to reproduce experimental results [17]. Treating D as a constant is similar to the dephasing strength used in a Büttiker probe. However, the mathematical framework of SCBA is, of course, different from that of the Büttiker probe method [19]. Furthermore, a rigorous

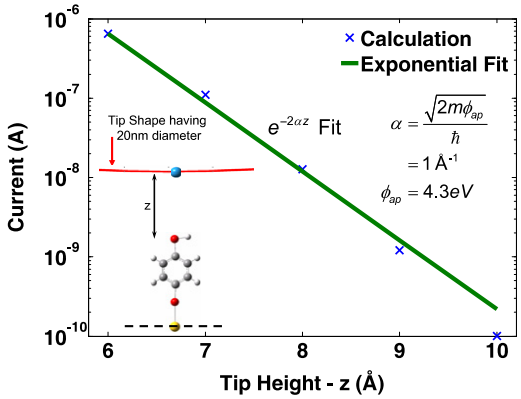

Figure 3. Tip modeling. The calculated current (I) for $V_{\text{tip}} = 1$ V as a function of tip–molecule distance (z) showing exponential dependence of current on z. The extracted barrier height from this I–z plot is 4.3 eV, whereas with the original parameters it is approximately 10 eV. The calculated apparent barrier height (ϕ_{ap}) is close to the work functions of the contacts being used. Furthermore, for calculating the Laplace and image potentials due to V_{tip}, a 20 nm diameter tip is used as shown in the inset. The tip is 7 Å away from the molecule in this visualization.

calculation of dephasing functions and dephasing strength can be readily incorporated in our model. Apart from this, SCBA has some limitations, e.g. it does not take care of multiple phonon processes implicitly for a single scattering event. It also does not include crossed diagrams which correspond to successive emission and re-absorption of phonons by the same electron.

We use a three-dimensional finite-element solver[1] for solving the Laplace equation in three dimensions to obtain the potential drop across the molecule due to V_{tip}. This method also provides the zero bias band line-up potential due to the Fermi level mismatch of 0.1 eV between Au(111) and W(110) tip, whose work functions are 5.1 and 5.2 eV, respectively. For $V_{\text{tip}} = 1$ V and 10 Å tip height, the HOMO level moves by about 0.15 eV due to the Laplace potential. We take the proper tip shape into account. A 20 nm tip diameter is assumed as shown in the inset of figure 3. The Hartree potential for the molecule is approximated via the complete neglect of the differential overlap method [22, 25]. Image effects are incorporated to include the correct barrier shape for vacuum tunneling [26] and to ensure that the Hartree self-consistency is not overestimated.

3. Tip modeling

For a good tip which can give atomic resolution, the last atom at the tip apex dominates STS. Therefore, we calculate the overlap between molecule and tip for this single tungsten atom. This assumption is for a tip without any adsorbate or multiple tip structures which may give ghost images in scanning tunneling microscopy (STM). We use the W(110) configuration since it is the lowest energy state. Furthermore, for working tip heights, electronic effects due to the wavefunction overlap between the tip atoms and the molecule become important. This overlap gives an exponential dependence of the decay of tunnel current (I) with tip height (z). Usually, it is agreed that, by changing tip height by 1 Å, current should change by an order of magnitude. This gives a barrier height of about 4–5 eV—close to the work functions of the materials being used. Within the WKB approximation, apparent barrier height (ϕ_{ap}) can be calculated from the slope of the $\log(I) - z$ plot. We find that the apparent barrier height is about 10 eV with unmodified EHT parameters, which is unphysical. We report a scheme for modifying the basis set of the tip atom to get the correct apparent barrier height. One does not need to modify the basis set of atoms in the molecule because they are already optimized for the gas phase. A similar approach has been used before in the context of scanning tunneling microscopy [27]. With the modified EHT parameters of the s-orbital basis set[2] for s tungsten atom, we obtain $\phi_{\text{ap}} = 4.3$ eV from the calculated $\log(I)$–z plot with $V_{\text{tip}} = 1$ V as shown in figure 3.

The above parameter modification affects S_1 and H_1, provided the tip self-energy Σ_1 is defined as $[(E + \text{i}0^+)S_1 - H_1]g_{\text{s1}}((E + \text{i}0^+)S_1^\dagger - H_1^\dagger)$, where g_{s1} is the surface Green's function for the tip. We assume a constant g_{s1}, calculated from the density of states at the equilibrium chemical potential of bulk tungsten $D_{\text{W}}(\mu_o)$, i.e. $g_{\text{s1}} = -\text{i}\pi D_{\text{W}}(\mu_o)$—a commonly used approximation (see, e.g., [17] and references therein). However, Σ_1 is still energy-dependent and this energy dependence should, in fact, capture all the barrier tunneling effects. However, it would not be able to capture the features due to the peculiar atomic and electronic structure of the tip as in [28].

4. Discussion of results

In this section, we apply the proposed EHT-NEGF-SCBA model to incoherent transport with elastic dephasing through the highest occupied molecular orbital (HOMO) level of a PDT/BDT molecule bonded to an Au(111) substrate through a single Au–S bond and probed using a tungsten W(110) tip as shown in figure 1. The Au–S bond length is the standard 2.53 Å and the tip–molecule distance is 10 Å. The dephasing strength (D) at 300 K is taken as 0.15 eV^2 to obtain experimentally observed broadening. Dephasing strength at any other temperature T is then calculated following equation (11).

The calculated I–V characteristics are shown in figure 4(a). For coherent conduction through the PDT/BDT molecule at 300 K ($D = 0$), the I–V curve has a sharp rise, which is consistent with the localized transmission peak in figure 5 for $D = 0$. Figure 4(b) provides an alternate view showing the $\text{d}I/\text{d}V$–V characteristics. The full width at half-maximum (FWHM) of the conductance peak is about 0.2 eV. This broadening is due to (1) the finite lifetime of electrons in the molecule as a result of the coupling with the contacts given by the broadening functions $\Gamma_{1,2}$, (2) contact Fermi functions giving about $5.4k_{\text{B}}T$ broadening and (3) the Hartree potential, which is small because the tip is 10 Å from the molecule.

[1] COMSOL is a trademark of COMSOL AB comsol.com.

[2] Original $\zeta = 2.341$, modified $\zeta = 1.104\,27$.

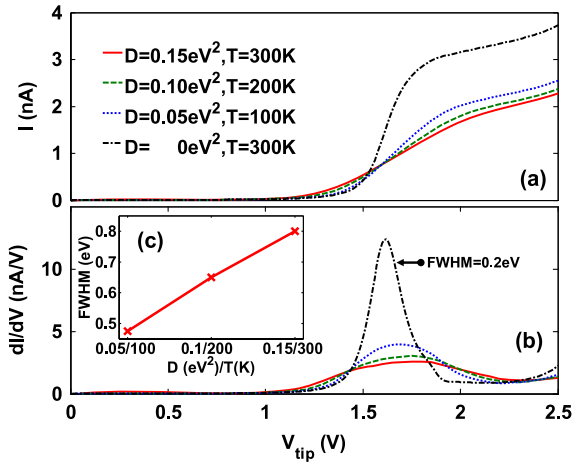

Figure 4. Incoherent resonant conduction through the highest occupied molecular orbital (HOMO) level with elastic dephasing due to low energy electron–phonon scattering. The dephasing strength (D) is directly proportional to the temperature (T). Thus, the additional broadening due to elastic dephasing decreases with decreasing temperature in a linear fashion. (a) I–V characteristics showing broadening of spectroscopic features due to dephasing. (b) dI/dV–V characteristics providing an alternate and more detailed view of broadening of spectroscopic features. (c) Full width at half-maximum (FWHM) of the first conductance peak corresponding to the HOMO level showing a linear dependence on temperature. The dephasing strength (D) is 0.15 eV^2 at 300 K to give experimentally observed broadening.

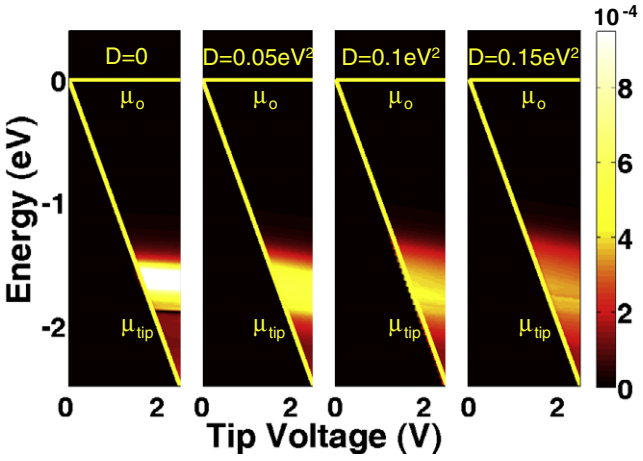

Figure 5. Incoherent non-equilibrium transmission through the HOMO level. The product of the transmission and Fermi function difference $[T(E)(f_1 - f_2)]$ is shown. Without dephasing ($D = 0$) at 300 K, the transmission peak is localized in energy. With increasing dephasing ($D = 0.05$ eV^2, 100 K; $D = 0.1$ eV^2, 200 K; $D = 0.15$ eV^2, 300 K), the transmission peak broadens due to spectral broadening.

With $D = 0.15$ eV^2 at 300 K, the I–V curve gets smeared out due to spectral broadening induced by elastic dephasing and overall current level and transmission decreases as shown in figures 4(a) and 5, respectively. The effect of spectral broadening on transmission is shown in figure 5 as well for varying dephasing strengths at different temperatures. Furthermore, for $D = 0.15$ eV^2, current starts increasing earlier and hence is slightly higher than in the $D = 0$ case for $V_{\rm tip} < 1.45$ V. Correspondingly, the dI/dV plot (see figure 4(b)) has a higher conductance value for 1.45 V $> V_{\rm tip} > 1.8$ V (i.e. before and after the conductance peak). The FWHM of this conductance peak is about 0.8 eV, as shown in figure 4(c). The additional 0.6 eV broadening is due to elastic dephasing. Such a high broadening has been observed experimentally[3]. Apart from this, the comparison of I–V and dI/dV–V plots for $D = 0$ and $D = 0.15$ eV^2 at 300 K raises two important questions: (1) why does the overall current value decreases and (2) how does the temperature dependence of dephasing strength affect the FWHM of the conductance peaks?

The answer to the first question depends on the energy dependence of the contact broadening functions $\Gamma_{1,2}$. After including dephasing, the spectral weight increases in the energy range where it was smaller before and vice versa. If the energy region, where the spectral weight is transferred, has larger broadening functions $\Gamma_{1,2}$, it results in a higher current. We analyze the energy dependence of $\Gamma_{1,2}$ and find that $\Gamma_{1,2}$ decrease as a function of decreasing energy, which corresponds to positive $V_{\rm tip}$. Thus, the broadened molecular spectral function gives rise to higher current values for lower $V_{\rm tip}$, where the broadening functions $\Gamma_{1,2}$ are larger. Similarly, current values are smaller for larger $V_{\rm tip}$, where $\Gamma_{1,2}$ are smaller. Hence, the overall current level decreases with dephasing. However, in a previous study [17] with n^{++}-H:Si(001)-(2 × 1) contact, we conclude that the overall current level increases with dephasing. In [17], the HOMO level is near the valence band edge, where the contact density of states (DOS) is small, resulting in a small current. After including dephasing, the HOMO level gets broadened and a portion of it is in the energy range where the DOS is large. Thus, dephasing in this case results in an order of magnitude higher current.

With decreasing temperature and dephasing strength, e.g. at 200 and 100 K with $D = 0.1$ and 0.05 eV^2 respectively, the I–V and transmission plots follow the same trend as shown in figures 4(a) and (b), and 5, respectively. The calculated FWHM values of these conductance peaks are shown in figure 4(c) to quantify the effect of dephasing. FWHM is directly proportional to the temperature and dephasing strength. The dependence of FWHM of the conductance peak on temperature and dephasing strength could become complex if temperature-dependent structural changes are present.

In figure 6, we report the inelastic tunneling spectroscopy (IETS) of the PDT/BDT molecule at 4 K. The purpose of these standard and well-established results is to convey the message that the model is able to handle calculations for inelastic dephasing as well. We assume a single phonon mode with energy $\hbar\omega = 75$ meV and emission dephasing function $D^{\rm em} = 0.1$ eV^2. The absorption dephasing function is then given as $D^{\rm ab} = D^{\rm em}{\rm e}^{-\hbar\omega/k_{\rm B}T}$. Figure 6(a) shows the I–V characteristics with no features of the IETS signal.

[3] See, for example, figure 4 in [29]—experimentally it is possible to extract information about FWHM only from the low bias half of the conductance peak, which gives an FWHM of more than an eV. Also, since the tip is far from the sample (about 1 nm away), the broadening due to Hartree self-consistency is expected to be small.

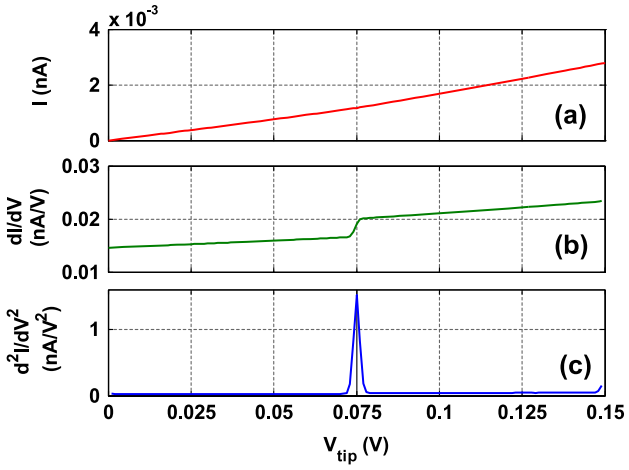

Figure 6. Effect of inelastic scattering on the off-resonant conduction at 4 K assuming one-phonon mode with $D^{\mathrm{em}} = 0.1$ eV^2 and $\hbar\omega = 75$ meV. (a) IETS signature is not noticeable in the I–V characteristics. (b) Inelastic scattering results in a step in the $\mathrm{d}I/\mathrm{d}V$–V characteristics. (c) IETS spectra ($\mathrm{d}^2I/\mathrm{d}V^2$–$V$ characteristics) showing a peak at 75 meV corresponding to the phonon mode. Since $\hbar\omega \gg k_{\mathrm{B}}T$, $D^{\mathrm{ab}} = D^{\mathrm{em}}\mathrm{e}^{-\hbar\omega/k_{\mathrm{B}}T} \approx 0$. Thus, the IETS peak is due to emission of phonons and processes due to the absorption of phonons are weak.

Figure 6(b) shows the $\mathrm{d}I/\mathrm{d}V$–V characteristics with a step in the conductance curve due to emission of phonons at $eV_{\mathrm{tip}} = \hbar\omega = 75$ meV. The same feature appears as a peak in the $\mathrm{d}^2I/\mathrm{d}V^2$ spectrum as shown in figure 6(c). Furthermore, we include the Hartree self-consistency for elastic dephasing only. Since IETS is usually studied in the off-resonance regime, the Hartree self-consistency is not important.

5. Conclusions

We have reported an EHT-NEGF-SCBA model and have used it to study elastic and inelastic dephasing. It has been previously reported that low lying modes are important in molecular conduction at low temperature [6, 10, 11, 15]. We suggest that they should be important at room temperatures as well and should be included in transport calculations. Furthermore, for $\hbar\omega \ll k_{\mathrm{B}}T$, inelastic dephasing can be approximated by elastic dephasing. Within this approximation, it can be shown that the broadening is proportional to temperature. Moreover, for Au contacts, the overall current level tends to reduce due to this dephasing. This could help bridge the gap between theory and experiment for resonant conduction along with other proposals [30], where theoretically calculated currents are higher as compared to the experimental observations [31]. Finally, we present results for IETS to show that, within the model, inelastic dephasing can be handled as well.

Acknowledgments

It is a pleasure to acknowledge useful discussions with S Datta and E C Kan. We thank F Zahid and T Z Raza for Hückel-IV 3.0 [22] codes and later for reviewing the manuscript. Computational facilities were provided by the NSF Network for Computational Nanotechnology.

References

[1] Raza H 2007 *Phys. Rev.* B **76** 045308
[2] Raza H, Edwin C and Kan E C 2008 *J. Comput. Electron.* **7** 372
[3] Raza H and Kan E C 2008 *Phys. Rev.* B **77** 245434
[4] Stipe B C, Rezaei M A and Ho W 1998 *Science* **280** 1732
[5] Wang W, Lee T, Kretzschmar I and Reed M A 2004 *Nano Lett.* **4** 643
[6] Kushmerick J G, Lazorcik J, Patterson C H, Shashidhar R, Seferosand D S and Bazan G C 2004 *Nano Lett.* **4** 639
[7] Wanga W and Richterb C A 2006 *App. Phys. Lett.* **89** 153105
[8] Troisi A, Beebe J M, Picraux L B, van Zee R D, Stewart D R, Ratner M A and Kushmerick J G 2007 *Proc. Natl Acad. Sci.* **104** 14255
[9] Frederiksen T, Brandbyge M, Lorente N and Jauho A-P 2004 *Phys. Rev. Lett.* **93** 256601
[10] Sergueev N, Roubtsov D and Guo H 2005 *Phys. Rev. Lett.* **95** 146803
[11] Chen Y-C, Zwolak M and Ventra M D 2005 *Nano Lett.* **5** 621
[12] Paulsson M, Frederiksen T and Brandbyge M 2006 *Nano Lett.* **6** 258
[13] Troisi A and Ratner M A 2005 *Phys. Rev.* B **72** 033408
[14] Galperin M, Ratner M A and Nitzan A 2007 *J. Phys.: Condens. Matter* **19** 103201
[15] Kato H S, Noh J, Hara M and Kawai M 2002 *J. Phys. Chem.* B **106** 9655
[16] Park H, Park J, Lim A K L, Anderson E H, Alivisatos A P and McEuen P L 2000 *Nature* **407** 57
[17] Raza H, Bevan K H and Kienle D 2008 *Phys. Rev.* B **77** 035432
[18] Dennington R II, Keith T, Millam J, Eppinnett K, Hovell W L and Gilliland R 2003 *GaussView, Version 3.0* (Shawnee Mission, KS: Semichem, Inc.)
[19] Datta S 2005 *Quantum Transport: Atom to Transistor* (Cambridge: Cambridge University Press)
[20] Zahid F, Paulsson M and Datta S 2003 Electrical conduction through molecules *Advanced Semiconductors and Organic Nano-techniques (III)* ed H Morkoc (San Diego, CA: Academic)
[21] Howell J, Rossi A, Wallace D, Haraki K and Hoffman R *FORTICON8, QCPE Program 545* Department of Chemistry, Cornell University, Ithaca, NY
[22] Zahid F, Paulsson M, Polizzi E, Ghosh A W, Siddiqui L and Datta S 2005 *J. Chem. Phys.* **123** 064707
[23] Meir Y and Wingreen N S 1992 *Phys. Rev. Lett.* **68** 2512
[24] Mahan G D 1987 *Phys. Rep.* **145** 251
[25] Pople J A and Segal G A 1996 *J. Chem. Phys.* **44** 3289
[26] Binnig G, Garcia N, Rohrer H, Soler J M and Flores F 1984 *Phys. Rev.* B **30** 4816
[27] Cerda J, Yoon A, Hove M A V, Sautet P, Salmeron M and Somorjai G A 1997 *Phys. Rev.* B **56** 15900
[28] Xue Y, Datta S, Hong S, Reifenberger R, Henderson J I and Kubiak C P 1999 *Phys. Rev.* B **59** R7852
[29] Tian W D, Datta S, Hong S H, Reifenberger R, Henderson J I and Kubiak C P 1998 *J. Chem. Phys.* **109** 2874
[30] Emberly E G and Kirczenow G 2001 *Phys. Rev. Lett.* **87** 269701
[31] Di Ventra M, Pantelides S T and Lang N D 2000 *Phys. Rev. Lett.* **84** 979